'iCycle-pBAO': Automated patient-specific beam-angle selection in proton therapy applied to oropharyngeal cancer

Kong, W.; Huiskes, M.; Habraken, S.J.M.; Astreinidou, E.; Rasch, C.R.N.; Heijmen, B.J.M.; Breedveld, S.

Radiotherapy and Oncology 206 (2025) 110799

Contents lists available at ScienceDirect

Radiotherapy and Oncology

journal homepage: www.thegreenjournal.com

Original Article

'iCycle-pBAO': Automated patient-specific beam-angle selection in proton therapy applied to oropharyngeal cancer

W. Kong [a,*], M. Huiskes [b], S.J.M. Habraken [b,c], E. Astreinidou [b], C.R.N. Rasch [b,c], B.J.M. Heijmen [a], S. Breedveld [a]

[a] Department of Radiotherapy, Erasmus MC Cancer Institute, Rotterdam University Medical Center, Rotterdam, the Netherlands
[b] Department of Radiation Oncology, Leiden University Medical Center, Leiden, the Netherlands
[c] HollandPTC, Delft, the Netherlands

A B S T R A C T

Objective: This study aimed to develop a fully-automated patient tailored beam-angle optimisation approach for intensity-modulated proton therapy (IMPT). For oropharynx cancer patients, the dosimetric impact of increasing the number of fields from 4 to 12 was systematically assessed.
Approach: A total-beam-space heuristic was developed to simultaneously select optimal patient specific candidate beam directions, according to a cost-function that penalises dose to OARs involved in clinically used NTCPs. The method was dosimetrically validated by comparisons with fixed 4- and 6-field clinical beam-angle templates and equiangular configurations, including 72-field equiangular. The latter served as dosimetric 'Utopia' benchmark for the other evaluated beam configurations.
Main result: Using 4 optimised patient-specific fields instead of the clinical 4-field beam-angle template resulted in (xerostomia NTCP + dysphagia NTCP)-reductions for all patients, with averages of 3.0 %-point (range: 1.1–5.8) for grade 2 toxicity and 1.2 %-point (range: 0.3–2.8) for grade 3. For 6 fields these reductions were 2.4 %-point (range: 0.0–5.0) and 0.8 %-point (range: −0.1–2.1). Xerostomia NTCPs significantly reduced with increasing numbers of patient-specific fields with a levelling off at 10–12 fields with NTCP values that closely approached those for Utopia 72-field equiangular plans. Beam angle optimisation took 52 min.
Conclusion: Automated, patient-tailored beam-angle optimisation could enhance IMPT plans at acceptable optimisation times. Improvements compared to the clinical beam-angle templates were highly patient-specific.

Introduction

Patient-specific beam-angle optimisation in proton therapy (proton BAO, 'pBAO') is a combinatorial problem with complex relationships between selected angles and optimal fluence profiles and resulting total doses. Manual iterative planning to establish optimal patient-specific angles can be a lengthy process with no guarantee of optimality in patient dose.

Clinical intensity modulated proton therapy (IMPT) practice often relies on predefined beam-angle templates for patient groups, established through manual planning for a small set of test patients. Per patient, small adjustments may be made to account for patient-specific anatomy (e.g., to avoid direct irradiation of part of an OAR). Unlike photon-based therapy, beam angles in IMPT are typically few [1], highlighting the significance of their selection. In principle, allowing more fields should result in plan improvements, but this may increase treatment time. Therefore, an increase in the number of applied fields must be justified by a clinically relevant increase in plan quality.

In both photon and proton therapy, performing an exhaustive beam-angle search for each patient is practically infeasible due to calculation times. For photon therapy, many alternative computerised BAO strategies have been suggested in the literature [2–19], whereas only a few studies have investigated pBAO. Gu et al.[20,21] used group sparsity regularisation, selecting only three to four fields. Results for two skull base tumour patients (4-field) and two bilateral head-and-neck patients (3-field) showed comparable plan robustness and better OAR sparing for pBAO compared to manual angles. Cao et al [22,23] proposed a local neighbourhood search algorithm in which each beam was exchanged with one of its neighbours to find the optimal configuration. Their method was applied to three prostate patients and two cases of skull-base chordoma. Two- to four-beam plans were optimised for prostate cases, and 2- and 3-field plans were optimised for skull base cases. For all plans with optimised angles, they observed improved target coverage and improved OAR sparing compared to a conventional two parallel-opposed fields plan [22]. For prostate cancer, optimised 3-field plans further improved rectum sparing over 2-field plans, while 4-field plans

* Corresponding author at: Dr. Molewaterplein 40, 3015 GD Rotterdam, the Netherlands.
E-mail address: w.kong@erasmusmc.nl (W. Kong).

https://doi.org/10.1016/j.radonc.2025.110799
Received 30 September 2024; Received in revised form 21 January 2025; Accepted 14 February 2025
Available online 28 February 2025

showed no advantage over 3-field [23]. Taasti et al.[24] proposed a Bayesian beam selection approach, using Bayesian optimisation to predict the treatment score for candidate beam angles not yet evaluated. Compared to the 2-field configurations for head-and-neck cancer (HN) patients chosen by the planner, the optimal 2-field configurations showed reductions in the mandible bone Dmax and in high doses in unspecified normal tissues [24]. Shen et al. [25] proposed an angle generation method to optimise IMPT plans with 2–4 fields. Their local search method iteratively optimised the angular set, performing group sparsity regularisation for the pivoting angle until the planning objective did not decrease further. For a candidate set of 24 beam angles, the algorithm provided nearly-exact solutions as an exhaustive search in a 2- and 4-field brain case, and a 3-field lung case [25].

Existing pBAO studies have involved limited numbers of patients (1–5) and fields (2–4). However, there is growing interest in exploring larger numbers of fields [26,27]. Currently, most HN cases in the Netherlands are treated with a 6-field class solution, and the DAHANCA 35 trial reported using 5 fields [28].

This study aimed to develop a fully-automated pBAO approach called 'iCycle-pBAO' for creating patient-specific coplanar multiple-beam configurations for oropharyngeal cancer patients. iCycle-pBAO starts with a total-beam-space plan [2], from which important beams are preselected to pick the requested number of beams. The method was dosimetrically validated by comparisons with clinical beam-angle templates and a 'best' equiangular configuration. The impact of increasing the number of fields from 4 to 12 was systematically investigated, with comparisons with 72-field equiangular IMPT as a Utopian dosimetric benchmark.

Methods and materials

This study was set up and executed following the RATING guidelines for treatment planning studies [29] and attained a score of 92 % (RATING score sheet in the supplementary material).

Patient data

Planning CT scans and delineations of ten randomly selected oropharynx cancer patients, previously treated with IMPT on a Varian ProBeam system (Varian, a Siemens Healthineers Company), were used. The data originate from the research database of the Holland Proton Therapy Centre. This database consists of data from all consenting patients treated at HollandPTC. The local Institutional Review Board waived the need to assess the protocol of the research database.

All patients were treated with a simultaneous integrated boost scheme, with 70 Gy_{RBE} prescribed to the primary tumour (CTV70) and 54.25 Gy_{RBE} to bilateral neck volumes and positive lymph nodes (CTV54.25), in accordance with our clinical practice.

Beam configuration selection and automated final plan generation – An overview

All plans in this study were generated through a two-step process: (1) selection of a co-planar beam configuration (patient-specific with iCycle-pBAO, equiangular or clinical template) and (2) automated generation of the final plan for the selected beam configuration (Fig. 1). Patient-specific coplanar beam configurations were selected using the proposed iCycle-pBAO. For validation of this approach, either an equiangular coplanar beam configuration or a clinical beam-angle template was selected in step 1.

In step 2, all final plans were generated using fully-automated multi-criteria plan generation as implemented in SISS-MCO [30], which has previously been validated against manual clinical planning [31]. SISS-MCO first establishes an optimal spot distribution for the pre-selected beam angles using Sparsity-Induced Spot Selection (SISS). The final dose is then optimised with automated Multi-Criteria Optimisation (MCO) as implemented in Erasmus-iCycle [3]. By design, final plans are Pareto-optimal regarding spot intensities.

Both SISS and MCO are wish-list driven. A wish-list defines a rule-based optimisation protocol with hard constraints and prioritised objectives. The same wish-list, aligned with clinical practice in our institution, was used for all patients and beam configurations, minimising bias in dosimetric comparisons. In line with clinical practice, both in iCycle-pBAO (Section 2.3) and in final plan optimisation (SISS-MCO [30]), beamlets that traversed the maxillary sinuses, shoulders and metal dental fillings were removed from the candidate spot sets and dose contributions per field were constrained to 47 Gy. All isocentres were placed at the centre of mass of CTV54.25. All plans had 3.5 mm energy layer spacing and 1 mm spot spacing in the candidate set.

iCycle-pBAO: Automated patient-specific beam configuration selection

iCycle-pBAO features a total-beam-space [2] optimisation approach for generating optimal patient-specific N-field beam-angle configurations in IMPT. First, a total-beam-space plan is optimised with all N_{tot} (72 in this study) candidate coplanar beam directions using a dedicated pBAO cost-function. Beams are then ranked by their target dose contribution. Next, beam angles for the final N-field plan are selected based on the highest target dose contributions and field separation (details below). Finally, the N-field plans are generated using the previously proposed SISS-MCO (Section 2.2).

The cost-function used to generate the total-beam-space plan (Eq. (1) was similar to the one used for beam spot selection with SISS (Kong et. al. [30]), with two key differences. Firstly, only a subset of OARs from the wish-list was considered. Secondly, the sparsity inducement consisted of a group sparsity norm $||x||_{1,2}$ to encourage grouping of spot weights for a field, while L_1 sparsity minimised the number of fields.

The cost-function comprised quadratic under- and overdose objectives (Q_i) for targets, overdose objectives for target shells, weighted

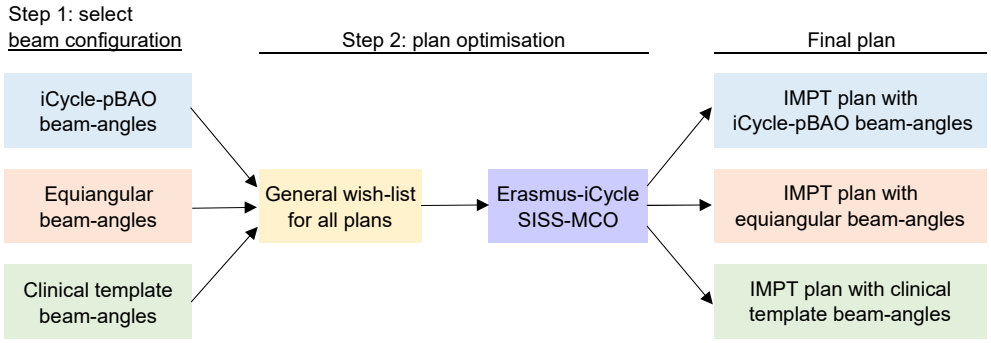

Fig. 1. Diagram showing the two-step plan generation process for all evaluated beam-angle configurations. See text for details.

mean dose functions for all considered OAR objectives, an L_1 for each beam direction b ($\lambda_1\|\boldsymbol{x}_b\|_1$), and a group sparsity inducement norm ($L_{1,2}$ norm: $\lambda_2\|\boldsymbol{x}\|_{1,2}$).

$$\underset{\boldsymbol{x}}{\text{minimise}} \sum_{i=1}^{N_Q} \mathrm{Q}_i(\boldsymbol{x}) + \sum_{j=1}^{N_\Lambda} w_M \bullet \mathrm{DMean}_j(\boldsymbol{x}) + \sum_{b=1}^{N_B} \lambda_1\|\boldsymbol{x}_b\|_1 + \lambda_2\|\boldsymbol{x}\|_{1,2} \tag{1}$$

$$\text{subject to } x \geq 0 \tag{2}$$

where

$\boldsymbol{x}$	=	spot weight vector
$\boldsymbol{x}_b$	=	spot weight vector belonging to beam direction b (zeros except for the indices of b)
N_Q	=	number of quadratic objectives
N_Λ	=	number of mean dose objectives
N_B	=	number of candidate beam directions
Q_i	=	quadratic objectives Eq. (3)
w_M	=	weighting coefficients for the mean dose objective Eq. (4)
DMean_j	=	mean dose objectives
λ_1	=	coefficient of the vector norm $= 10^{-6}$
λ_2	=	coefficient of the group sparsity norm $= 10^{-3}$

Quadratic penalties are defined in Eq. (3) where the value of M was chosen heuristically, based on experiments for three patients that were not used for validation. The values for D_{ref} were chosen in accordance with the prescription dose.

$$\mathrm{Q}_i(\boldsymbol{x}) = \frac{w_Q}{N_i}\mathrm{Q}_i\left(\boldsymbol{A}_i, \boldsymbol{x}, D_{ref}, M\right) = \frac{w_Q}{N_i}\sum_{k=1}^{N_i} \max\left(0, M(\boldsymbol{A}_{i;k}\boldsymbol{x} - D_{\mathrm{ref}})\right)^2 \tag{3}$$

where

N_i	=	number of voxels in structure i
D_{ref}	=	reference dose value
$\boldsymbol{A}_i$	=	dose deposition matrix for quadratic objectives i
$\boldsymbol{A}_{i;k}$	=	row k of dose deposition matrix $\boldsymbol{A}_i$
M	=	$\begin{cases} -10, \text{target underdose constraint} \\ 10, \text{target overdose constraint} \\ 1, \text{target overdose objective} \\ 0.1, \text{target shell overdose objective} \end{cases}$
w_Q	=	$\begin{cases} 1, \text{target constraint} \\ 0.5, \text{target objective} \\ 0.1, \text{target shell objective} \end{cases}$

Mean dose objectives were minimised for the subset of OARs that are related to NTCPs for xerostomia and dysphagia, in accordance with the Dutch National Protocol for Model-Based Selection for Proton Therapy in Head and Neck Cancer [32]. The relevant OARs for xerostomia were the left and right parotids, and the left and right submandibular glands. For dysphagia these were the oral cavity, and the inferior, middle, and superior pharyngeal constrictor muscles (PCM). The weighting coefficients for the OARs were determined using Eq. (4), which penalises an OAR objective inversely proportional to the volume $\boldsymbol{V}$ of overlap between the OAR in the nominal robustness scenario and the composite high-dose target in all 21 robustness scenarios (details on robustness scenarios in Section 2.4) to encourage OAR sparing where possible.

$$w_m = 100 \bullet \left(1 - \frac{\boldsymbol{V}_{\text{OAR inside target}}}{\boldsymbol{V}_{\text{OAR}}}\right) \tag{4}$$

Target dose contributions were used for ranking of beams in the total-beam-space plan, using Eq. (5).

$$\text{Importance beam direction } b = \sum_{l=1}^{N_{targets}} \sum_{i=1}^{N_i} \boldsymbol{A}_i\boldsymbol{x}_b \tag{5}$$

where

N_{targets}	=	number of targets (2 in this study)
N_i	=	number of voxels in structure i
$\boldsymbol{A}_i$	=	dose deposition matrix for target i
$\boldsymbol{x}_b$	=	spot weight vector belonging to beam direction b

The total-beam-space problem was solved using the L-BFGS-B [33–35] solver with non-negativity constraints for the spot intensity. The optimisations were performed on a computer node equipped with an Intel Xeon Gold 6248R @3.00 GHz CPU and an NVIDIA A100 GPU.

Beams in the total-beam-space plan with contribution (Eq. (5)) less than the median were removed from the ranked beam-angle set. For generation of an N-field plan, the N beam angles with the highest target dose contributions in the total-beam-space plan were selected, while maintaining at least $180/N^\circ$ spacing between all beam angles if possible, to ensure sufficient separation between angles. For 6 fields, a minimum of 30° separation was in line with our clinical practice. The minimum requested spacing of $180/N^\circ$ was reduced if the ranked set did not contain a solution that satisfied this spacing. With this approach, the set of angles selected for the N-field final plan did not necessarily contain the angles for final plans with $< N$ fields.

For the total-beam-space optimisation problem, dose deposition matrices for 144.000 candidate spots in the $N_{\mathrm{tot}} = 72$ candidate beams (2000 spots per beam direction) were calculated for all structures using the ASTROID dose engine [36]. Range shifters with 34 mm water-equivalent thickness were included in all fields where the lowest energy could not cover the most proximal target voxels. All spots were positioned in a volume consisting of the composite of the CTVs in all robustness scenarios, enlarged by 5 mm. Inside this volume, for each beam, energy layers were automatically selected considering the volume and the pre-defined energy layer spacing (3.5 mm). Spots were laterally sampled uniformly in all energy layers, where the lateral spacing within an energy layer was equal to the setting in the final plan.

Details for final plan generations with SISS-MCO

Minimum and maximum doses for both targets, and maximum doses for the brainstem, spinal cord, cochlea, optic nerves, optic chiasm, lenses, and mandible bone were optimised with scenario-based robust optimisation [37] using the following 21 scenarios: the nominal scenario (1 scenario), proton range undershoot and overshoot scenarios of 3 % in the absence of setup errors (2 scenarios), setup errors of 3 mm in positive and negative directions along three axes without range error (6 scenarios), and with undershoot (6 scenarios) and overshoot (6 scenarios) of 3 %. Non-robust mean dose minimisation was used for the following OARs: parotids, submandibular glands, inferior/middle/superior PCM, larynx supraglottic, glottic area, esophagus, cricopharyngeus, brainstem, and spinal cord. Clinical minimum and maximum monitor unit constraints were always adhered to.

Validation of iCycle-pBAO

Two approaches were used to validate iCycle-pBAO. First, 4-field and 6-field iCycle-pBAO plans were dosimetrically compared to corresponding SISS-MCO plans for our previous (4-field) and current (6-field) clinical beam-angle templates. These 4-field and 6-field templates consisted of the following (gantry, couch) angles: {(150°, 0°), (60°, 0°), (300°, 0°), (210°, 0°)} and {(200°, 0°), (260°, 20°), (310°, 0°), (50°, 0°), (100°, 340°), (160°, 0°)}. Second, 6-field coplanar iCycle-pBAO plans were compared to so called 'best' equiangular 6-field plans. For each patient, this 'best' plan was established by generating six 6-field equiangular plans with 10° rotations as a naive approach to explore the beam space. The configuration with the lowest sum of NTCPs for grade 2 and 3 xerostomia and dysphagia was defined as best-performing.

As in clinical practice, a range shifter with 34 mm water-equivalent thickness was inserted in all clinical template fields, except for the 160° and 200° gantry angles in the 6-field template. For 6-field and 72field equiangular configurations, range shifters were automatically inserted, if needed to cover the most proximal target voxels, similar to the use of range shifters in iCycle-pBAO plans, see Section 2.3.

Plan quality as a function of number of applied IMPT fields

For all study patients, iCycle-pBAO was used to select optimal configurations with 4-, 6-, 7-, 8-, 10 and 12-fields, followed by final IMPT plan generations with SISS-MCO. The latter plans were mutually compared to assess dependence of dosimetric plan quality on field number. For each *N*-field patient plan, the dosimetric metrics and NTCPs were presented as differences with the corresponding 72-field equiangular benchmark. For each patient, the 72-field benchmark was generated without restrictions on the number of energy layers. Therefore, while clinically infeasible to deliver due to the substantial number of fields and energy layers, they demonstrate the Utopian dosimetric potential for each patient.

Plan evaluations and comparisons

To ease the analyses, all generated plans were normalised such that CTV70 $D_{98\%}$ in the 21-scenario voxelwise minimum dose distribution [38] (VWmin) was equal to 95 % of the prescription dose, as requested clinically.

NTCPs for grade 2 (G2) and grade 3 (G3) xerostomia and dysphagia were determined according to the Dutch National Protocol for Model-Based Selection for Proton Therapy in Head and Neck Cancer.

Reported D_{mean} were calculated in the nominal scenario, and near-maximum doses were derived from voxel-wise maximum dose distributions [38] in accordance with clinical practice. Differences were tested for significance ($p < 0.05$) using two-sided Wilcoxon signed-rank tests.

All presented box plots have boxes that represent interquartile ranges (IQR) of dosimetric/NTCP differences with the horizontal bar indicating the median. Whiskers include all differences except for outliers, defined as: outside Q1–1.5 · IQR and Q3 + 1.5 · IQR.

Results

iCycle-pBAO took on average 52 min per patient (range: 34–77 min), excluding spot dose computations and data loading on GPU (see Discussion). The times for the subsequent generation of the final plan with SISS-MCO were around 2–4 h using a GPU and 2x20 core CPU, where about half of the computation time accounts for optimisation and the other half for dose computations [39].

All generated plans (for iCycle-pBAO and all other fixed beam configurations) met the clinical target and OAR hard constraints applied in our institution. For all plans, CTV70 VWmin $D_{98\%}$ was exactly 95.0 %, due to applied normalisation (Section 2.7), but also for CTV54.25 requested coverage was always obtained (VWmin $D_{98\%} \geq 95$ %).

Fig. 2 shows for two selected patients the 4-field and 6-field iCycle-pBAO (hereafter denoted as 'pBAO') gantry angles, the clinical templates, and the corresponding dose distributions. For patient 1 (upper panel), pBAO resulted in improved low-dose baths in the oral cavity and mandible. Patient 2 (lower panel), benefited from improved dose gradients in the left parotid gland, the mandible bone, and around CTV54.25. Notably, pBAO and clinical angles differed significantly for both patients.

Fig. 3 shows substantial interpatient differences between pBAO selected beam-angle configurations for all patients. For comparison, gantry angles for the clinical template, and for 'best' 6-field equiangular configuration are also presented.

Fig. 4 shows that pBAO plans were dosimetrically superior compared to 4-field and 6-field clinical templates and the best 6-field equiangular. While pBAO plans showed comparable target coverage as corresponding clinical template plans, lower doses to NTCP-related OARs were observed. For the fifteen OAR dose metrics presented in the upper panel of Fig. 4, median dose differences >0.5 Gy in favour of pBAO when compared to clinical templates, were observed for 11/15 OARs in 4-field comparisons and for 12/15 OARs when comparing 6-field plans. For only 3/15 and 1/15 OARs the clinical 4- and 6-field templates were favourable. For several parameters, median advantages of pBAO were modest, but whiskers and outliers pointed at larger advantages of pBAO for individual patients. A similar pattern was observed in the comparison of 6-field pBAO with best 6-field equiangular. Dosimetric advantages of pBAO translated in NTCP advantages (lower panel Fig. 4) with average improvements in (xerostomia G2 NTCP + dysphagia G2 NTCP), abbreviated as ΣNTCPG2, of 3.0 %-point (range: 1.1–5.8, $p = 0.002$) and 2.4 %-point (range: 0.0–5.0, $p = 0.004$) compared to 4-field and 6-field clinical templates, respectively. For ΣNTCPG3, these differences were 1.2 %-point (range: 0.3–2.8, $p = 0.01$) and 0.8 %-point (range: −0.1–2.1, $p = 0.004$). In terms of ΣNTCPG2, 4-field pBAO outperformed the 4-field clinical template in 10/10 cases. When comparing 6-field plans, pBAO compared favourably with both the clinical template and with best equiangular in 9/10 cases. The NTCP data in the lower panel of Fig. 3 point at large advantages of pBAO for a subgroup of patients. Trend analysis showed that pBAO had a larger benefit for patients with smaller CTV volumes. No statistically significant differences between pBAO and the clinical templates were observed in integral dose (data not shown).

Figs. 5 and 6 show the impact of increasing number of fields from 4 to 12 on pBAO plan quality. For most OAR dose metrics, the median value decreased with an increasing number of fields (Fig. 5), with some levelling off at 10 fields. In terms of NTCPs, the use of more fields, up to and including 10 fields, significantly improved the treatment plan in terms of xerostomia G2 and G3 (Fig. 6). Especially for 8–12 fields, differences with 72-field Utopia plans were small.

Significant reductions in integral dose were observed for 6/7/8/10/12/72-field plans compared to 4field, with a mean relative reduction of 5.6 % ($p = 0.03$) compared to 4-field. Addition of fields to 7–12 fields did not produce significant differences in the integral dose compared to 6-field pBAO. For the 72field benchmark, the integral dose reduced by 11.1 % ($p = 0.002$) compared to 4-field and 5.5 % ($p = 0.004$) compared to 6-field. For an example patient, Appendix A shows all chosen gantry angles and the corresponding importance score.

Discussion

This study introduced a fully-automated beam-angle optimisation approach for IMPT, called 'iCycle-pBAO'. For each patient, beam-angle optimisation starts with generating a total-beam-space plan [2], where all 72 candidate beam directions are optimised simultaneously according to a cost function that penalises dose to OARs involved in NTCPs, inversely proportional to their overlapping volume with the high-dose CTV. For a requested *N*-field plan, the best performing *N* fields, chosen with sufficient spacing, are then used for final wish-list based multi-criteria plan generation. The approach was demonstrated on ten patients with oropharyngeal cancer. All final plans in this study, i.e. with iCycle-pBAO based patient-specific beam angles or fixed angles, were automatically generated with the same wish-list to ensure the same dosimetric trade-offs and to eliminate manual planning bias. This study investigates beam-angle optimisation for up to 12-field treatments. To our knowledge, this is more than presented in literature on computerised BAO for IMPT, with a maximum of 4 fields. This is also the first study with a consistent patient population (oropharynx) with 10 cases included. Published studies have fewer cases and often more patient groups included.

Plans based on iCycle-pBAO beam configurations significantly outperformed plans based on clinical beam-angle templates in terms of ΣNTCPG2 and ΣNTCPG3. For 6-field treatments, ΣNTCPG2 and

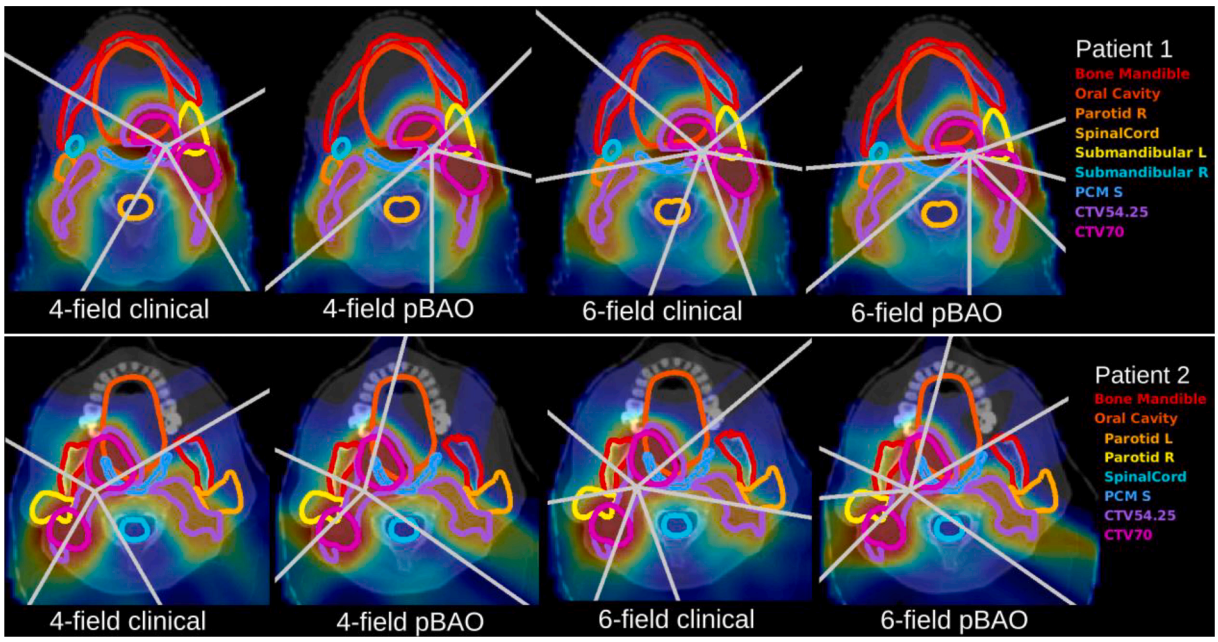

Fig. 2. Dose distributions and gantry angles for 2 patients for 4-field and 6-field clinical templates and pBAO. Patient 1 (upper panel): the patient with CTV70 + CTV54.25 vol closest to the mean, and patient 2 (lower panel): the patient with the smallest CTV70 volume.

Fig. 3. Gantry angles for the 6-field clinical template (first column), pBAO plans for patients 1–10 (columns 2–11) and 'best' 6-field equiangular setup (last column).

ΣNTCPG3 reduced by on average 2.4 %-point and 0.8 %-point compared to the clinical templates, with reductions up to 5.0 %-point and 2.1 %-point, indicating that gain of individualised beam angles may be highly clinically relevant for individual patients. iCycle-pBAO could also allow more patients to be eligible for proton therapy in the Netherlands as the ΔNTCP thresholds are 15 %-point and 7.5 %-point for grade 2 and 3 toxicity.

In this study we found that plan quality of iCycle-pBAO plans went gradually up with increasing numbers of beams up to around 10 fields. An open question is the added-value of 10-field iCycle-pBAO compared to 10-field equiangular. To investigate this, we generated for each of the ten included study patients a 10-field equiangular plan with beam angles {0°, 36°, 72°, 108°, 144°, 180°, 216°, 252°, 288°, 324°}. For 10-field equiangular and iCycle-pBAO, improvements in NTCP were observed in 9/10 and 10/10 cases respectively compared to the 6-field clinical template configuration. The average difference between 10-field equiangular and iCycle-pBAO in ΣNTCPG2 was −0.52 %-point (range:−3.7–1.15, $p = 0.04$) in favour of iCycle-pBAO. No significant differences were observed for ΣNTCPG3.

The experiments using iCycle-pBAO to systematically investigate plan quality as a function of the number of applied patient-specific IMPT beam directions showed that xerostomia NTCPs reduced by adding more fields, approaching the NTCP values for 72-field equiangular Utopia plans with 10–12 fields (Fig. 6). For dysphagia, increasing the number of fields did not result in systematic NTCP reductions (Fig. 6). In our clinic, xerostomia reduction has highest priority. This is reflected in the applied optimisation wish-list with highest priority for reduction of mean doses in xerostomia related OARs (parotids and submandibular glands according to the applied NTCP model [32]). Accordingly, the extra degrees of freedom resulting from adding fields was primarily used to reduce

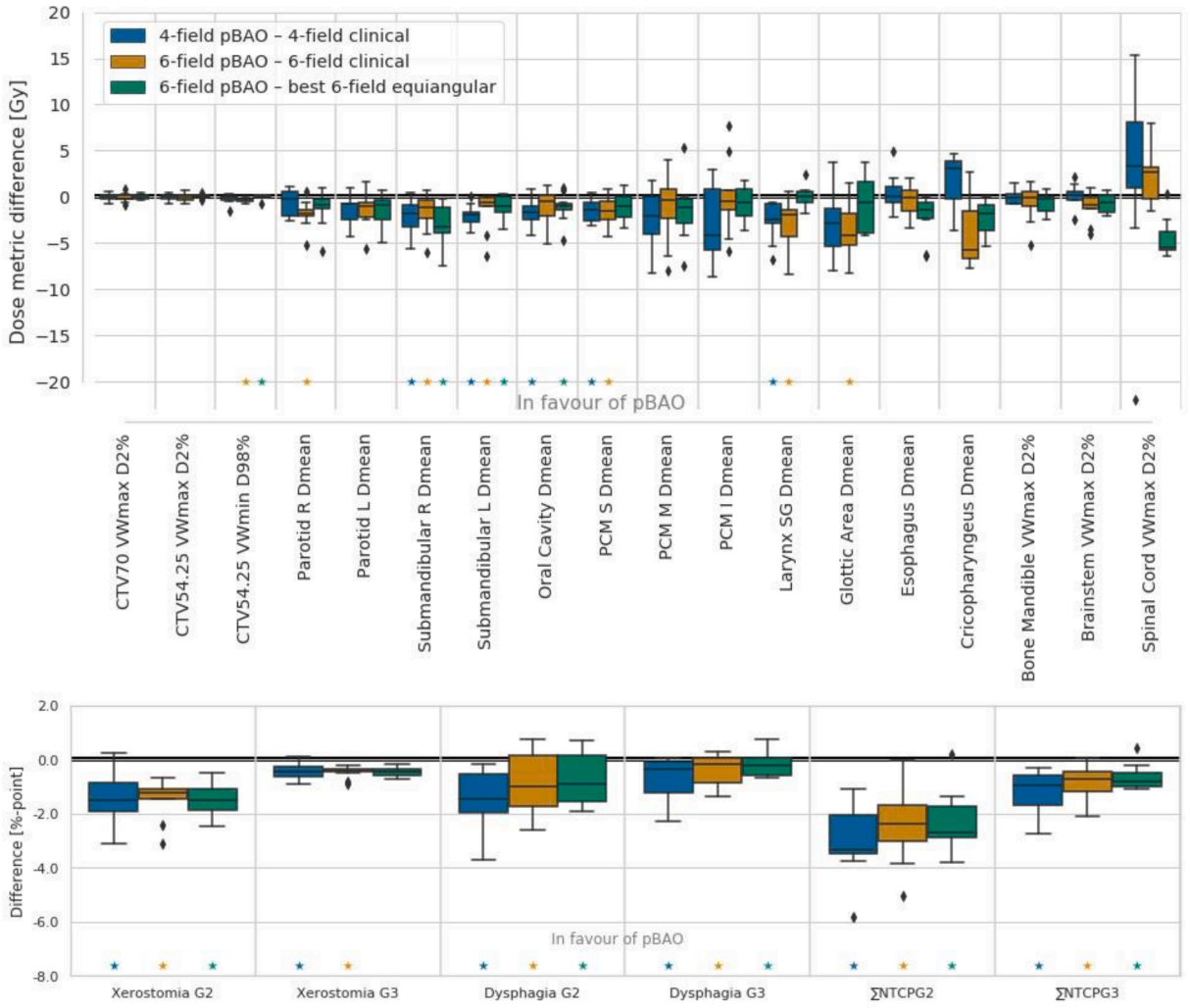

Fig. 4. Dose metric differences in the upper panel, and in the lower panel NTCP differences between pBAO and the clinical 4- and 6-field templates, and between 6-field pBAO and the best performing 6-field equiangular configuration (see Section 2.5 for details). Significant differences ($p < 0.05$) are indicated by asterisks. PCM = pharyngeal constrictor muscle.

mean doses in these OARs (Fig. 5). For dysphagia, calculated NTCPs depended on oral cavity, and inferior (I), middle (M) and superior (S) pharyngeal constrictor muscles (PCM) mean doses [32]. Fig. 5 shows that with increasing numbers of fields, oral cavity mean dose was practically constant, PCM S mean dose increased slightly and PCM M and PCM I showed a trend towards slight mean dose reductions. Apparently, this mix resulted in the observed independence of dysphagia NTCP of field number.

Optimised beam configurations were derived through automated optimisation without manual intervention or post-processing in on average 52 min. However, this does not include dose calculation times. In this study, we applied the ASTROID research dose engine [36] for this purpose, which is relatively slow [30]. Application of fast GPU-based [40–42] or deep learning-based [43] dose engines would further enhance usability of iCycle-pBAO in clinical workflows.

Taasti et al. [24] reported for their BAO approach a mean dose reduction of 2.3 Gy in the parotids for their five 2-field HN cases, while other NTCP-involved OARs were not investigated. Gu et al. [20] reported mean OAR dose differences between pBAO and manual beam angles ranging from −10.5 to +11.48 Gy for two 3-field HN cases. In this study, the added value of more fields was assessed as the majority of HN patients who receive IMPT in the Netherlands are treated with 6 fields; studies on low numbers of fields such as 2 or 3 would have had less clinical relevance. On the other hand, we also compared 4-field treatments (as clinically used up to a few years ago) with 6-field treatments, confirming that the recent increase to 6-field indeed resulted in improved NTCPs.

In this paper, we demonstrated that with the proposed pBAO approach, current IMPT quality can be significantly increased without additional cost. On the contrary: due to the automation, workload can be reduced. Recently, discrete and dynamic proton arc therapy (PAT) have obtained increasing attention in the literature [44–70]. Ding et al. [44] reported mean dose reductions in the parotid and submandibular glands using an 84-field dynamic arc strategy compared to 4-field IMPT for an oropharyngeal case. Wuyckens et al. [66] reported reductions up to 7.5 and 5.0 Gy for a dynamic 340-field plan with a single energy layer per field compared to 4-field IMPT. In our study, reductions of up to 5.7 and 11.3 Gy were observed between clinical 4-field and 72-field IMPT, while the reductions were 5.0 and 9.4 Gy for 4-field clinical template compared to 6-field pBAO. This may indicate that using only 6–8 well-selected beam angles could enhance dosimetry to the level of full arc therapy, while avoiding delivery issues in dynamic arc therapy. Further research is needed before final conclusions on this can be drawn. De Jong et al. [62] investigated 30-field step-and-shoot arc, where 360 energy layers were deployed. Again, comparisons were made only with 4-field clinical plans.

Discrete PAT has already been commissioned for clinical use [71]. The faster dynamic approach is not yet commercially available for

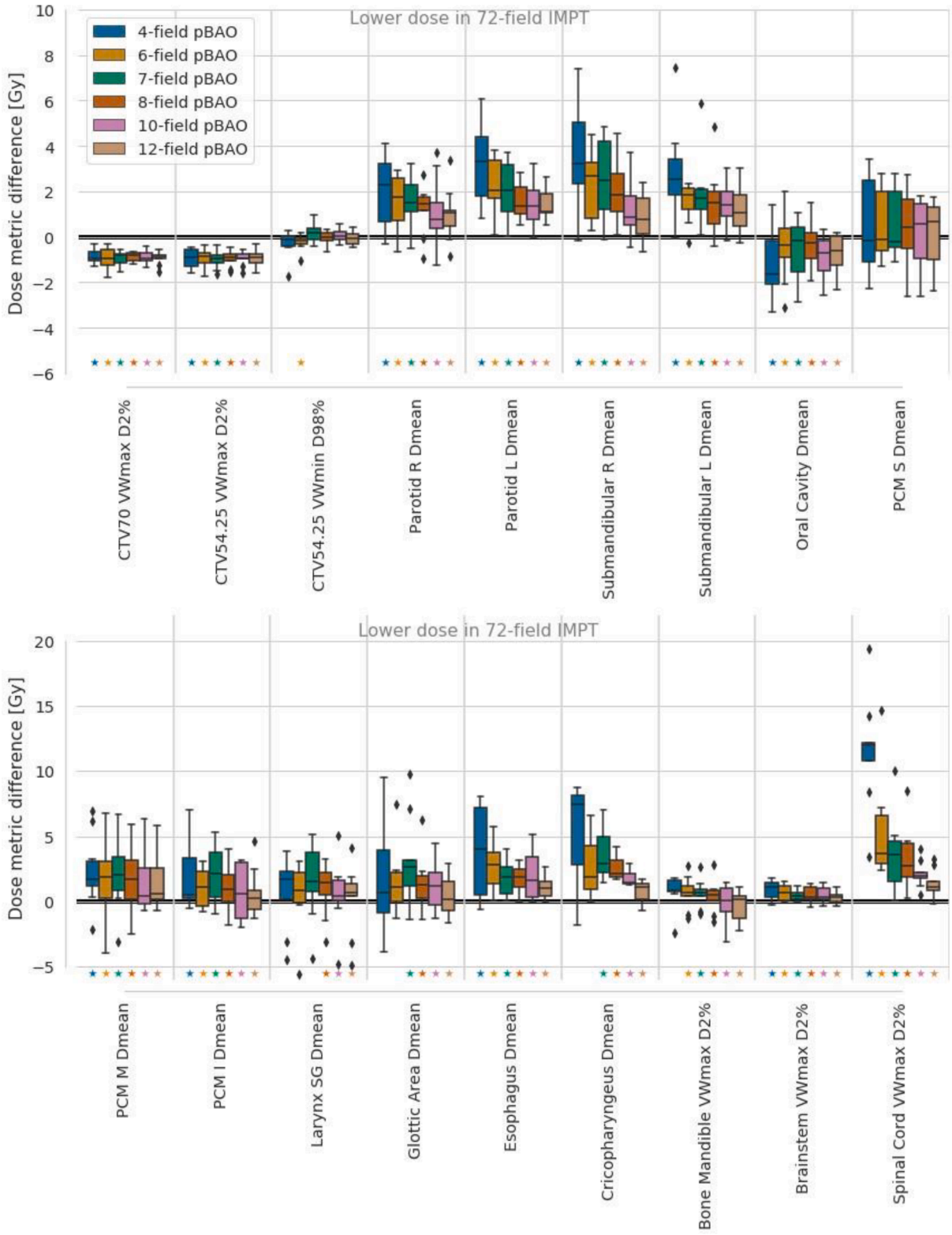

Fig. 5. Dose metric differences between 4–12 field pBAO plans and the 72-field Utopian plan benchmark. Significant differences ($p < 0.05$) are indicated by asterisks. PCM = pharyngeal constrictor muscle.

clinical use, as there are still technical challenges to overcome [72]. For both static and dynamic PAT, dosimetric gain is still a topic of active research. We believe that the automatically generated iCycle-pBAO plans with individualised 6–12 beam angles can serve as high-quality benchmark to assess the dosimetric advantages of PAT, instead of the currently much applied manually generated clinical template plans with often 4 fields or less. As can be seen in Fig. 6, NTCPs for 8–12 field iCycle-pBAO plans closely approached NTCPs for our 72-field equiangular benchmark plans. Dynamic PAT has no limitation in number of gantry angles, but it needs restrictions in e.g. the number of energy layers to keep delivery times acceptable. It is yet to be determined whether, and then to what extent, dynamic PAT would be able to

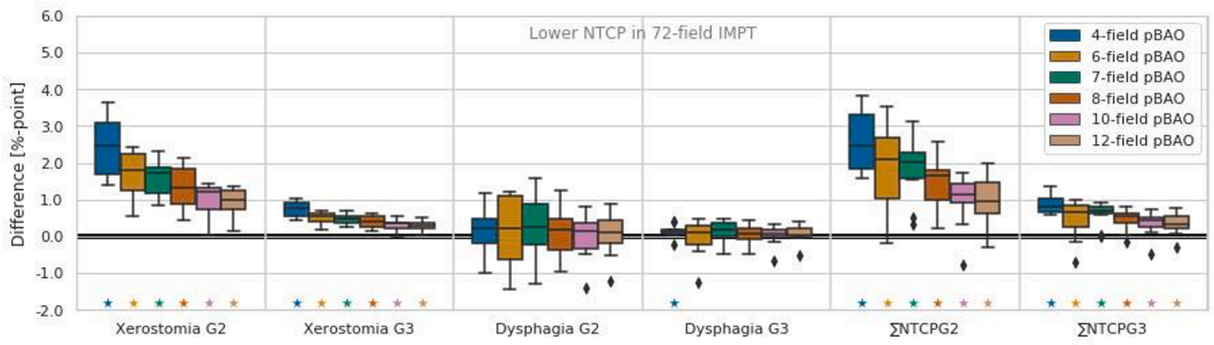

Fig. 6. For *N*-field plans, NTCP differences with respect to corresponding 72-field benchmark plans. Significant differences ($p < 0.05$) are indicated by asterisks.

approach or even improve on the NTCPs of 72-field benchmark plans that do not have such limitations. Another important parameter that has to be considered in comparisons between iCycle-pBAO and PAT is the delivery time.

Deep learning approaches relying on training data with manually chosen beam angles have also been proposed for IMPT pBAO [73–75]. Often the aim of the deep learning approach is to be non-inferior to the manually chosen beam configuration whereas in optimisation approaches, the aim is to outperform manual beam configurations.

This study has several limitations. One limitation is that we have validated iCycle-pBAO exclusively in oropharyngeal cancer patients. Investigation is needed for other treatment sites. In this work, iCycle-pBAO was driven by OAR penalties that were inversely proportional to their overlap with the high-dose CTV. For other treatment sites where overlap never occurs, a different metric should be used to weigh the OAR penalties. Distance metrics are among the logical candidates. Other study limitations were that only coplanar beam configurations were considered, and that it was for each included field upfront decided whether or not to use a range shifter. The total-beam space approach in iCycle-pBAO features many degrees of freedom by optimising all candidate beams simultaneously, but is very memory intensive for the same reason. Expansion of the candidate beam set by the addition of non-coplanar fields and fields with and without range shifters was not possible on the hardware used. Pencil beams that would cross the patient's shoulders were excluded to allow for some inter-fraction uncertainty, in line with clinical practice (Section 2.4). However, in our institution, two fields in the 6-field clinical template are slightly non-coplanar (20° coach rotation) to create extra safety for shoulder positioning. Possibly, clinical usage of our iCycle-pBAO plans would require 3D optical imaging to ensure proper positioning of shoulders. Future research could incorporate non-coplanar fields.

In conclusion, a novel algorithm for automated patient-tailored beam-angle optimisation in IMPT was presented. For oropharynx patients, plans with patient-specific, optimised beam angles were dosimetrically superior to plans with fixed clinical beam angles, with large interpatient variations. Optimisation times allow application in clinical routine. When increasing the number of optimised fields from 4 to 12, dosimetric plan quality levelled off at around 10 fields, approaching quality of 72-field equiangular Utopia plans.

CRediT authorship contribution statement

W. Kong: Writing – review & editing, Writing – original draft, Visualization, Validation, Software, Methodology, Investigation, Formal analysis, Data curation, Conceptualization. **M. Huiskes:** Writing – review & editing. **S.J.M. Habraken:** Writing – review & editing, Supervision, Conceptualization. **E. Astreinidou:** Writing – review & editing, Conceptualization. **C.R.N. Rasch:** Writing – review & editing, Funding acquisition, Conceptualization. **B.J.M. Heijmen:** Writing – original draft, Writing – review & editing, Validation, Project administration, Investigation, Conceptualization, Funding acquisition, Methodology. **S. Breedveld:** Writing – review & editing, Writing – original draft, Validation, Supervision, Software, Methodology, Investigation, Funding acquisition, Conceptualization.

Funding

The research for this work was funded by Varian, a Siemens Healthineers Company and partly funded by the Surcharge for Top Consortia for Knowledge and Innovation (TKIs) from the Dutch Ministry of Economic Affairs and Climate.

Declaration of competing interest

The authors declare that they have no known competing financial interests or personal relationships that could have appeared to influence the work reported in this paper.

Appendix A. Supplementary material

Supplementary data to this article can be found online at https://doi.org/10.1016/j.radonc.2025.110799.

References

[1] Mohan R, Grosshans D. Proton therapy–present and future. *Adv Drug Deliv Rev* 2017;109:26–44.
[2] Schipaanboord B, Heijmen B, Breedveld S. Tbs-bao: Fully automated beam angle optimization for imrt guided by a total-beam-space reference plan. *Phys Med Biol* 2022;67(3):035004.
[3] Breedveld S, Storchi PR, Voet PW, Heijmen BJ. Icycle: Integrated, multicriterial beam angle, and profile optimization for generation of coplanar and noncoplanar imrt plans. *Med Phys* 2012;39(2):951–63.
[4] Bedford JL, Ziegenhein P, Nill S, Oelfke U. Beam selection for stereotactic ablative radiotherapy using cyberknife with multileaf collimation. *Med Eng Phys* 2019;64:28–36.
[5] Bangert M, Unkelbach J. Accelerated iterative beam angle selection in imrt. *Med Phys* 2016;43(3):1073–82.
[6] Lim GJ, Choi J, Mohan R. Iterative solution methods for beam angle and fluence map optimization in intensity modulated radiation therapy planning. *OR Spectr* 2008;30(2):289–309.
[7] Aleman DM, Kumar A, Ahuja RK, Romeijn HE, Dempsey JF. Neighborhood search approaches to beam orientation optimization in intensity modulated radiation therapy treatment planning. *J Glob Optim* 2008;42:587–607.
[8] D'Souza WD, Meyer RR, Shi L. Selection of beam orientations in intensity-modulated radiation therapy using single-beam indices and integer programming. *Phys Med Biol* 2004;49(15):3465.
[9] Li Y, Yao J, Yao D. Automatic beam angle selection in imrt planning using genetic algorithm. *Phys Med Biol* 2004;49(10):1915.
[10] Wang X, Zhang X, Dong L, Liu H, Wu Q, Mohan R. Development of methods for beam angle optimization for imrt using an accelerated exhaustive search strategy. *Int J Radiat Oncol* Biol* Phys* 2004;60(4):1325–37.
[11] Meedt G, Alber M, Nüsslin F. Non-coplanar beam direction optimization for intensitymodulated radiotherapy. *Phys Med Biol* 2003;48(18):2999.
[12] Lee EK, Fox T, Crocker I. Integer programming applied to intensity-modulated radiation therapy treatment planning. *Ann Oper Res* 2003;119:165–81.
[13] Djajaputra D, Wu Q, Wu Y, Mohan R. Algorithm and performance of a clinical imrt beam-angle optimization system. *Phys Med Biol* 2003;48(19):3191.

[14] Hou Q, Wang J, Chen Y, Galvin JM. Beam orientation optimization for imrt by a hybrid method of the genetic algorithm and the simulated dynamics. *Med Phys* 2003;30(9):2360–7.
[15] Das S, et al. Beam orientation selection for intensity-modulated radiation therapy based on target equivalent uniform dose maximization. *Int J Radiat Oncol* Biol* Phys* 2003;55(1):215–24.
[16] Pugachev A, et al. Role of beam orientation optimization in intensity-modulated radiation therapy. *Int J Radiat Oncol* Biol* Phys* 2001;50(2):551–60.
[17] Haas O, Burnham K, Mills J. Optimization of beam orientation in radiotherapy using planar geometry. *Phys Med Biol* 1998;43(8):2179.
[18] Stein J, et al. Number and orientations of beams in limintensity-modulated radiation treatments. *Med Phys* 1997;24(2):149–60.
[19] Bortfeld T, Schlegel W. Optimization of beam orientations in radiation therapy: Some theoretical considerations. *Phys Med Biol* 1993;38(2):291.
[20] Gu W, Neph R, Ruan D, Zou W, Dong L, Sheng K. Robust beam orientation optimization for intensity-modulated proton therapy. *Med Phys* 2019;46(8):3356–70.
[21] Gu W, et al. Integrated beam orientation and scanning-spot optimization in intensity-modulated proton therapy for brain and unilateral head and neck tumors. *Med Phys* 2018;45(4):1338–50.
[22] Cao W, et al. Uncertainty incorporated beam angle optimization for impt treatment planning. *Med Phys* 2012;39(8):5248–56.
[23] Cao W, Lim GJ, Li Y, Zhu XR, Zhang X. Improved beam angle arrangement in intensity modulated proton therapy treatment planning for localized prostate cancer. *Cancers* 2015;7(2):574–84.
[24] Taasti VT, Hong L, Shim JS, Deasy JO, Zarepisheh M. Automating proton treatment planning with beam angle selection using bayesian optimization. *Med Phys* 2020;47(8):3286–96.
[25] Shen H, Zhang G, Lin Y, Rotondo RL, Long Y, Gao H. Beam angle optimization for proton therapy via group-sparsity based angle generation method. *Med Phys* 2023;50(6):3258–73.
[26] Ödén J, Toma-Dasu I, Witt Nyström P, Traneus E, Dasu A. Spatial correlation of linear energy transfer and relative biological effectiveness with suspected treatment-related toxicities following proton therapy for intracranial tumors. *Med Phys* 2020;47(2):342–51.
[27] Shang H, et al. Impact of multiple beams on plan quality, linear energy transfer distribution, and plan robustness of intensity modulated proton therapy for lung cancer. *ACS Sensors* 2020;6(2):408–17.
[28] Hansen CR, et al. Evaluation of decentralised model-based selection of head and neck cancer patients for a proton treatment study. dahanca 35. *Radiother Oncol* 2024;190:109812.
[29] Hansen CR, et al. Radiotherapy treatment planning study guidelines (rating): A framework for setting up and reporting on scientific treatment planning studies. *Radiother Oncol* 2020;153:67–78.
[30] Kong W, et al. Siss-mco: Large scale sparsity-induced spot selection for fast and fully-automated robust multi-criteria optimisation of proton plans. *Phys Med Biol* 2024.
[31] Huiskes M, et al. Validation of fully automated robust multicriterial treatment planning for head and neck cancer impt. *Int J Radiat Oncol* Biol* Phys* 2024. issn: 0360-3016.
[32] National Association for Radiotherapy in the Netherlands, "Landelijk indicatieprotocol protonentherapie hoofdhals v2.2.," 2019. [Online]. Available: https://nvro.nl/images/documenten/rapporten/2019-08-15_Landelijk_Indicatieprotocol_Protonentherapie_Hoofdhals_v2. 2.pdf.
[33] Byrd RH, Lu P, Nocedal J, Zhu C. A limited memory algorithm for bound constrained optimization. *SIAM J Sci Comput* 1995;16(5):1190–208.
[34] Zhu C, Byrd RH, Lu P, Nocedal J. Algorithm 778: L-bfgs-b: Fortran subroutines for largescale bound-constrained optimization. *ACM Transactions on mathematical software (TOMS)* 1997;23(4):550–60.
[35] Morales JL, Nocedal J. Remark on "algorithm 778: L-bfgs-b: Fortran subroutines for largescale bound constrained optimization". *ACM Transactions on Mathematical Software (TOMS)* 2011;38(1):1–4.
[36] Kooy HM, et al. A case study in proton pencil-beam scanning delivery. *Int J Radiat Oncol* Biol* Phys* 2010;76(2):624–30.
[37] Fredriksson A, Forsgren A, Hårdemark B. Minimax optimization for handling range and setup uncertainties in proton therapy. *Med Phys* 2011;38(3):1672–84.
[38] Korevaar EW, et al. Practical robustness evaluation in radiotherapy–a photon and proton-proof alternative to ptv-based plan evaluation. *Radiother Oncol* 2019;141:267–74.
[39] Kong W, et al. Reducing the lateral dose penumbra in impt by incorporating transmission pencil beams. *Radiother Oncol* 2024:110388.
[40] Jia X, Schümann J, Paganetti H, Jiang SB. Gpu-based fast monte carlo dose calculation for proton therapy. *Phys Med Biol* 2012;57(23):7783.
[41] Ma J, Beltran C, Seum Wan Chan Tseung H, Herman MG. A gpu-accelerated and monte carlo-based intensity modulated proton therapy optimization system. *Med Phys* 2014;41(12):121707.
[42] Wan Chan Tseung H, Ma J, Beltran C. A fast gpu-based monte carlo simulation of proton transport with detailed modeling of nonelastic interactions. *Med Phys* 2015;42(6 Part1):2967–78.
[43] Pastor-Serrano O, Perkó Z. Millisecond speed deep learning based proton dose calculation with monte carlo accuracy. *Phys Med Biol* 2022;67(10):105006.
[44] Ding X, Li X, Zhang JM, Kabolizadeh P, Stevens C, Yan D. "Spot-scanning proton arc (sparc) therapy: The first robust and delivery-efficient spot-scanning proton arc therapy. *Int J Radiat Oncol* Biol* Phys* 2016;96(5):1107–16.
[45] Ding X, et al. Have we reached proton beam therapy dosimetric limitations?–a novel robust, delivery-efficient and continuous spot-scanning proton arc (sparc) therapy is to improve the dosimetric outcome in treating prostate cancer. *Acta Oncol* 2018;57(3):435–7.
[46] Toussaint L, et al. Towards proton arc therapy: physical and biologically equivalent doses with increasing number of beams in pediatric brain irradiation. *Acta Oncol* 2019;58(10):1451–6.
[47] Ding X, et al. Improving dosimetric outcome for hippocampus and cochlea sparing whole brain radiotherapy using spot-scanning proton arc therapy. *Acta Oncol* 2019;58(4):483–90.
[48] Carabe A, et al. Radiobiological effectiveness difference of proton arc beams versus conventional proton and photon beams. *Phys Med Biol* 2020;65(16):165002.
[49] Bertolet A, Carabe A. Proton monoenergetic arc therapy (pmat) to enhance letd within the target. *Phys Med Biol* 2020;65(16):165006.
[50] Liu G, et al. A novel energy sequence optimization algorithm for efficient spot-scanning proton arc (sparc) treatment delivery. *Acta Oncol* 2020;59(10):1178–85.
[51] Liu G, et al. Improve the dosimetric outcome in bilateral head and neck cancer (hnc) treatment using spot-scanning proton arc (sparc) therapy: A feasibility study. *Radiat Oncol* 2020;15:1–11.
[52] Gu W, Ruan D, Lyu Q, Zou W, Dong L, Sheng K. A novel energy layer optimization framework for spot-scanning proton arc therapy. *Med Phys* 2020;47(5):2072–84.
[53] Chang S, et al. Feasibility study: Spot-scanning proton arc therapy (sparc) for left-sided whole breast radiotherapy. *Radiat Oncol* 2020;15:1–11.
[54] Li X, et al. Linear energy transfer incorporated spot-scanning proton arc therapy optimization: a feasibility study. *Front Oncol* 2021;11:698537.
[55] Liu G, et al. Lung stereotactic body radiotherapy (sbrt) using spot-scanning proton arc (sparc) therapy: a feasibility study. *Front Oncol* 2021;11:664455.
[56] Liu G, et al. Is proton beam therapy ready for single fraction spine sbrs?–a feasibility study to use spot-scanning proton arc (sparc) therapy to improve the robustness and dosimetric plan quality. *Acta Oncol* 2021;60(5):653–7.
[57] Zhao L, Liu G, Li X, Ding X. An evolutionary optimization algorithm for proton arc therapy. *Phys Med Biol* 2022;67(16):16NT01.
[58] Wuyckens S, et al. Bi-criteria pareto optimization to balance irradiation time and dosimetric objectives in proton arc therapy. *Phys Med Biol* 2022;67(24):245017.
[59] Engwall E, et al. Fast robust optimization of proton pbs arc therapy plans using early energy layer selection and spot assignment. *Phys Med Biol* 2022;67(6):065010.
[60] Zhang G, Long Y, Lin Y, Chen RC, Gao H. A treatment plan optimization method with direct minimization of number of energy jumps for proton arc therapy. *Phys Med Biol* 2023;68(8):085001.
[61] Liu G, et al. Development of a standalone delivery sequence model for proton arc therapy. *Med Phys* 2023.
[62] de Jong BA, et al. Proton arc therapy increases the benefit of proton therapy for oropharyngeal cancer patients in the model based clinic. *Radiother Oncol* 2023;184:109670.
[63] De Jong BA, et al. Spot scanning proton arc therapy reduces toxicity in oropharyngeal cancer patients. *Med Phys* 2023;50(3):1305–17.
[64] Engwall E, et al. Partitioning of discrete proton arcs into interlaced subplans can bring proton arc advances to existing proton facilities. *Med Phys* 2023;50(9):5723–33.
[65] Henjum H, et al. Influence of beam pruning techniques on let and rbe in proton arc therapy. *Front Oncol* 2023;13:1155310.
[66] Wuyckens S, et al. Efficient proton arc optimization and delivery through energy layer pre-selection and post-filtering. *Med Phys* 2024.
[67] Zhu Y-N, et al. Proton arc based lattice radiation therapy: Feasibility study, energy layer optimization and let optimization. *Phys Med Biol* 2024;69(21):215027.
[68] Wase V, Marthin O, Fredriksson A, Finnson A. Optimizing the traversal time for gantry trajectories for proton arc therapy treatment plans. *Phys Med Biol* 2024;69(6):065007.
[69] Ma J, Zhu Y, Lin Y, Tang M, Gao H. Enhancing proton arc treatment efficiency with a multi-arc approach. *Int J Radiat Oncol Biol Phys* 2024;120(2):S110.
[70] Chocan MS, et al. A dosimetric and robustness analysis of proton arc therapy with early energy layer and spot assignment for lung cancer versus conventional intensity modulated proton therapy. *Acta Oncol* 2024;63:40549.
[71] Fracchiolla F, et al. Static proton arc therapy: Comprehensive plan quality evaluation and first clinical treatments in patients with complex head and neck targets. Med Phys 2025. https://doi.org/10.1002/mp.17669.
[72] Mein S, et al. Particle arc therapy: Status and potential. *Radiother Oncol* 2024:110434.
[73] Kaderka R, et al. Toward automatic beam angle selection for pencil-beam scanning proton liver treatments: a deep learning–based approach. *Med Phys* 2022;49(7):4293–304.
[74] Kaderka R, Huang Y, Lo H, Tu Y, Chang C. Ai beam angle prediction in proton therapy for brain patients. *Int J Radiat Oncol Biol Phys* 2023;117(2):e470.
[75] R. Bellotti, N. Bizzocchi, A. J. Lomax, A. Adelmann, D. C. Weber, and J. Hrbacek, "Gambas–fast beam arrangement selection for proton therapy using a nearest neighbour model," *arXiv preprint arXiv:2408.01206*, 2024.